THE JOURNAL OF PHYSICAL CHEMISTRY B

Article

pubs.acs.org/JPCB

DNA−Gelatin Complex Coacervation, UCST and First-Order Phase Transition of Coacervate to Anisotropic ion gel in 1-Methyl-3-octylimidazolium Chloride Ionic Liquid Solutions

Kamla Rawat,[†] V. K. Aswal,[‡] and H. B. Bohidar[†,*]

[†]Polymer and Biophysics Laboratory, School of Physical Sciences, Jawaharlal Nehru University, New Delhi 110067, India

[‡]Solid State Physics Division, Bhabha Atomic Research Centre, Mumbai 400094, India

Supporting Information

ABSTRACT: Study of kinetics of complex coacervation occurring in aqueous 1-octyl-3-methylimidazolium chloride ionic liquid solution of low charge density polypeptide (gelatin A) and 200 base pair DNA, and thermally activated coacervate into anisotropic gel transition, is reported here. Associative interaction between DNA and gelatin A (GA) having charge ratio (DNA:GA = 16:1) and persistence length ratio (5:1) was studied at fixed DNA (0.005% (w/v)) and varying GA concentration (C_{GA} = 0−0.25% (w/v)). The interaction profile was found to be strongly hierarchical and revealed three distinct binding regions: (i) Region I showed DNA-condensation (primary binding) for C_{GA} < 0.10% (w/v), the DNA ζ potential decrease from −80 to −5 mV (95%) (partial charge neutralization), and a size decrease by ≈60%. (ii) Region II (0.10 < C_{GA} < 0.15% (w/v)) indicated secondary binding, a 4-fold turbidity increase, a ζ potential decrease from −5 to 0 mV (complete charge neutralization), which resulted in the appearance of soluble complexes and initiation of coacervation. (iii) Region III (0.15 < C_{GA} < 0.25% (w/v)) revealed growth of insoluble complexes followed by precipitation. The hydration of coacervate was found to be protein concentration specific in Raman studies. The binding profile of DNA-GA complex with IL concentration revealed optimum IL concentration (=0.05% (w/v)) was required to maximize the interactions. Small angle neutron scattering (SANS) data of coacervates gave static structure factor profiles, $I(q)$ versus wave vector q, that were remarkably similar and invariant of protein concentration. This data could be split into two distinct regions: (i) for 0.0173 < q < 0.0353 Å^{-1}, $I(q) \sim q^{-\alpha}$ with α = 1.35−1.67, and (ii) for 0.0353 < q < 0.35 Å^{-1}, $I(q) = I(0)/(1 + q^2\xi^2)$. The correlation length found was ξ = 2 ± 0.1 nm independent of protein concentration. The viscoelastic length (≈8 nm) was found to have value close to the persistence length of the protein (≈10 nm). Rheology data indicated that the coacervate phase resided close to the gelation state of the protein. Thus, on a heating−cooling cycle (heating to 50 °C followed by cooling to 20 °C), the heterogeneous coacervate exhibited an irreversible first-order phase transition to an anisotropic ion gel. This established a coacervate−ion gel phase diagram having a well-defined UCST.

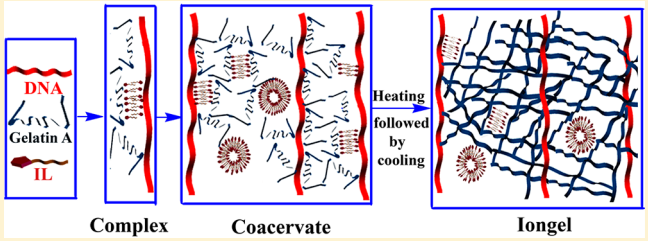

I. INTRODUCTION

Intermolecular associative interaction between oppositely charged macromolecules, which is mostly driven by electrostatic forces, often leads to liquid−liquid phase separation (called coacervation transition).[1−8] Here a homogeneous solution separates into a polymer-rich phase (called coacervate) and it is supernatant. Coacervation usually involves the spontaneous formation of a superdense liquid phase from a homogeneous macromolecular solution of poor solvent affinity.[1−3] In complex coacervation, the loss of solvation that leads to phase separation arises from the interaction of complementary macroion species. The formation of such macromolecule-rich fluids is well-known in mixtures of complementary polyelectrolytes; it can also occur from mixtures of polyelectrolytes with colloidal particles, leading to condensed phases that are associated with interesting properties. Properties of such self-assembled coacervates can be varied continuously from those of homogeneous liquids, to viscous gel-like materials, and finally to amorphous solids, without protein denaturation.[9,10] Complex coacervates and the accompanied process of self-organization of oppositely charged macroions are ubiquitous in nature. Some examples of these are underwater glue of the sandcastle worm,[11] the bacterial nucleoid,[12,13] and chromatin fibers of the DNA−histone complexes.[14−16] Strong electrostatic interactions and hydration present in coacervate materials provide a delicate balance that is expected to yield interesting soft matter phases. Nguyen and Shklovskii[17] examined the phase diagram of DNA and positively charged colloidal macroions in dispersion and observed the following: (i) at low colloid concentration, the DNA−colloid complexes are negatively charged with DNA wrapping the colloids, whereas (ii) at high colloid concen-

Received: October 16, 2012
Revised: November 28, 2012
Published: November 29, 2012

tration, the complexes showed charge reversal and revealed positive charge. The aforesaid two situations are separated by an intermediate phase where the complexes are fully charge-neutralized; here DNA−colloid condensates exist. Therefore, the concentration of colloidal macroions governed the condensation and reentrant condensation in this system. This has been discussed in further detail in the literature.[18−25] Fine tuning the controlling parameters like the solution pH, temperature, ionic strength, and hydrophobicity can alter the microscopic structure and property of these materials, thereby generating tailormade products for specific applications.[26−29]

Proteins can interact with DNA either specifically or nonspecifically. In the case of nonspecific interactions, the sequence of nucleotides does not matter, as far as the binding interactions are concerned. Histone (protein)−DNA interactions are an example of such interactions, and they occur between functional groups on the protein and the sugar−phosphate backbone of DNA. Specific DNA−protein interactions, however, depend upon the sequence of bases in the DNA and on the orientation of the bases that can vary with twisting and supercoiling. These DNA−protein interactions are strong, and are mediated by (i) hydrogen bonding, (ii) ionic interactions like formation of salt bridges, protein side chains−DNA backbone interaction, and (iii) van der Waal and hydrophobic interactions. Such interactions can produce novel biomaterials and investigation of such systems aid to our general understanding of soft matter.

Ionic liquids (ILs) are salts composed of poorly coordinating organic cations and inorganic anions that are liquid below the boiling point of water. They possess appealing features such as low melting points, negligible vapor pressure, nonvolatility, inflammability, wide electrochemical windows, and so on.[30−34] Ionic liquids are often referred to as "designed solvents" because their physical properties could be tailored by adjusting the structure and species of the constituting cations and/or anions. These materials are gaining sufficient attention in the recent past in the field of chemical and process engineering. The variety of possible combinations of anions and cations can, in principle, generate a wide spectrum of green solvents.[35] This necessitates a clear understanding of intermolecular hydrogen bonding, Coulombic, hydrophobic and vander Waal interactions occurring in these systems. Thus, molecular interactions in the solutions of ILs are significantly different from those in water. The low dilution liquid−liquid phase equilibria of some ILs have been established.[36]

Interaction of ILs with cellulose, nucleic acids, and proteins has generated considerable interest in the recent past.[37] For instance, room temperature ionic liquid 1-octyl-3-methylimidazolium chloride stabilizes protein dispersions over a wide range of solution pH.[38] Similarly, nucleic acids have been shown to remain in stable dispersion at room temperature in IL solutions.[37] This raises a pertinent question: how is the DNA−protein interaction altered in IL solutions vis a vis in water? This constitutes the main objective of the present work. More specifically, we have chosen DNA and gelatin A, a low charge density polypeptide, and systematically studied their interaction profile over a wide range of protein and IL concentration using an array of experimental techniques. Further the microscopic structure of the complex coacervates formed of the two biopolymers was probed using small angle neutron scattering (SANS) and rheology. Because complex coacervates are dense phases of oppositely charged macroions containing large amount of water of hydration, the same was investigated by Raman spectroscopy. The results revealed two interesting conclusions: (i) there exists a hierarchy in DNA−protein intermolecular interaction and (ii) on exposure to a heating−cooling cycle, the amorphous coacervate material undergoes an irreversible first-order phase transition to an anisotropic protein ion gel phase with DNA molecules supporting the structure as scaffolds.

II. MATERIALS AND METHODS

In this study, IL refers to [C8mim][Cl]. Gelatin A in powder form and 1-methyl-3-octylimidazolium chloride ([C8mim]-[Cl]) in immensely viscous form were bought from Sigma-Aldrich and used as received. DNA (200 bp) was procured from Acros Organics, respectively, and used as received. Gelatin A (300 bloom) from porcine skin had maximum nominal impurities as follows: sulfate ash = 1.5%; $SO_2 = 2 \times 10^{-4}$% and heavy metals (Zn, Cu, Pb) in the concentration lower than the SO_2 concentration. This preparation was devoid of any *Escherichia coli* and liquefier presence. It needs to be mentioned that the protein was not subjected to further purification by dialysis, which would have made it salt free. Both the biopolymers had comparable molecular weight. Stock of gelatin A (GA) solution was prepared by dissolving known amount of the protein in double distilled deionized water at 40 °C using a magnetic stirrer for almost 1 h. DNA stock was prepared by dissolving DNA powder in double distilled deionized water at room temperature and mixed for an hour. Both the solutions appeared optically clear and transparent after preparation. Final samples for experiment were prepared by mixing gelatin A and DNA solution from their stock, appropriate dilution was used to achieve exact mixing ratio. In all the stock solutions the DNA concentration was maintained at 0.005% (w/v) and the gelatin A concentrations were varied from $C_{GA} = 0$ to 0.25% (w/v). The pH of the stock solution (=6.0 ± 0.5) remained invariant of GA or IL concentration. These samples were stored in airtight borosilicate glass bottles for further analysis which, in all instances, did not exceed more than 48 h after preparation. All procedures were performed at room temperature, 20 °C, and the relative humidity in the room was less than 50%. Two sets of experiments were carried out, namely investigation of DNA-GA interaction at a fixed IL but with different GA concentration, and study of the same at a fixed GA but with different IL concentration. Coacervates were extracted from reacted solutions following standard procedure of repeated centrifugation and decantation of the supernatant.[3−6] To the best of our knowledge this is the only and commonly used method for extraction of coacervate from reacting solution. It has been observed that, when the same protocol is used for the coacervate extraction, the physical properties do not change from sample to sample. Gels made in IL solutions are referred to as ion gels and their corresponding sols as ion sols in this work.

The extent of aggregation (resulting from intermolecular interaction) was inferred through quantitative measurement of solution turbidity to support light scattering and electrophoresis data. The change in transmittance (%T) was monitored continuously using a colorimeter (Brinkmann-910, Brinkmann Instruments) operating at 450 nm. A UV−vis spectrophotometer (Model CE-7300, Cecil Instruments) was used to carry out absorbance measurements. The solution viscosity was measured using a vibro viscometer (model-SV10, A and D Co.). This instrument uses a matched pair of gold plated flat electrodes. The mechanical vibrations (frequency ≈30 Hz) set

dx.doi.org/10.1021/jp3102089 | J. Phys. Chem. B 2012, 116, 14805−14816

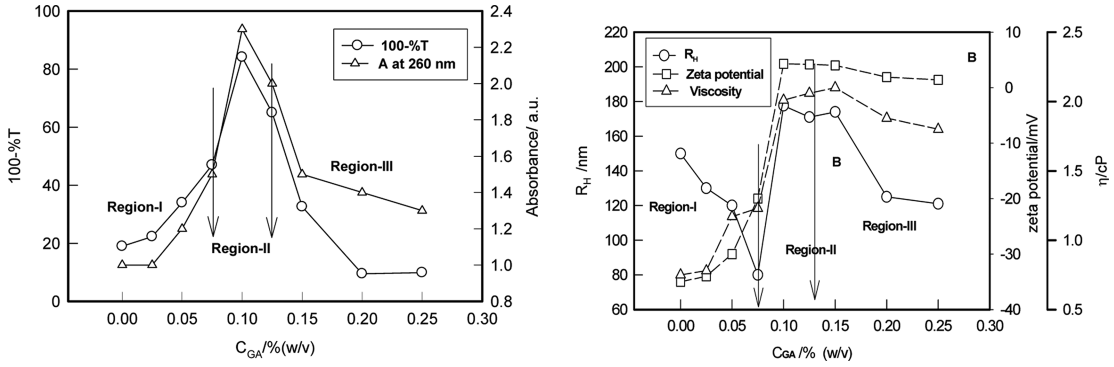

Figure 1. (A) Gelatin A concentration dependent variation of solution turbidity (100-%T) and absorbance A at 260 nm and (B) hydrodynamic radii, ζ potential, and viscosity in IL solutions. Here, DNA and IL concentrations were fixed at 0.005 and 0.05% (w/v), respectively. Solid lines are guides to the eye. Arrows demarcate various binding zones. See text for details.

in one of these propagate through the sample and are picked up by the detector electrode. The viscosity is determined from the analysis of the response function recorded by this electrode using the software provided by the manufacturer. With this technique, the product of the viscosity and density is directly measured. With such low frequency (30 Hz) and dilute concentration of sample, shear rate effects are negligible and density can be assumed to be constant.

The zeta potential (ζ) measurements of sample solution were performed on an electrophoresis instrument (ZC-2000, Microtek). The electrostatic property of a macroion can be described through its mobility μ or ζ potential. This is given by the Smoluchowski equation, $\zeta = 4\pi\eta\mu/\varepsilon$. The ζ potential is the potential felt at the hydrodynamic slip plane of a uniformly charged sphere is given by $\zeta = 4\pi\sigma/\varepsilon\kappa$, where σ is the surface charge density of the particle and ε and κ are the dielectric constant and the Debye–Huckel parameter of the solution respectively.[39,40] The said relationships are normally proposed for spherical charged colloidal particles dispersed in a polar medium. This equation provides a clear and linear link between surface charge and ζ potential. However, in general, the ζ potential manifested by a macroion is a complicated function of its geometry and surface charge density[39,40] and further discussion on this will be out of context for the present work.

Small angle neutron scattering (SANS) requires a neutron source, i.e., a nuclear reactor or an accelerator-based spallation source, and therefore, the experiments are performed at large scale facilities. The small angle neutron scattering experiments presented in this work have been performed at the SANS diffractometer at the Guide Tube Laboratory, Dhruva Reactor, Bhabha Atomic Research Centre, India.[41] It makes use of polycrystalline block of beryllium oxide (BeO) filter as monochromator. The mean wavelength of the monochromatic beam was 5.2 Å with a spread of $\Delta\lambda/\lambda \sim 15\%$. The angular distribution of neutrons scattered by the sample was recorded using a 1m long one-dimensional He position sensitive detector. The instrument covered a q-range of 0.015–0.35 Å^{-1}.

DLS experiments on the sample solutions were performed at scattering angle of $\theta = 90°$ and laser wavelength of $\lambda = 632.8$ nm using a commercial correlator (Model: RiNa, NabiTech GmbH) that was operated in the multi-τ mode (logarithmically spaced channels). The instrument was placed on a Newport vibration isolation table. In this method, the system has refractive index n and is physically seen over a length scale q^{-1} where $q = (4\pi n/\lambda)\sin\theta/2$. The laser wavelength in the scattering medium is λ/n. The translational diffusion coefficient D is related to corresponding apparent hydrodynamic radius R_h through Stoke–Einstein relation as

$$D = k_B T/(6\pi\eta_0 R_h) \quad (1)$$

where solvent viscosity is η_0, k_B is the Boltzmann constant, and T is absolute temperature.

The particle size was obtained from the correlation functions using CONTIN regression analysis software provided by the instrument supplier.

Rheological measurements, using small amplitude oscillatory shear, were performed on the IL–water samples using controlled stress AR 500 rheometer (TA Instruments, Surrey, England). For all the tests, the storage modulus (G') data were computed from raw dynamic oscillatory data using TA Instrument Rheology Advantage Data Analysis software (version 3.0.1). All measurements were performed in triplicate to ensure data reproducibility (relative standard deviation less 5%) for each sample. Rheology experiments were performed with the objective to interrelate the stiffness and thermal stability of the networks in frequency and temperature sweep modes. In the frequency sweep experiments, coacervate samples of different GA concentrations were loaded onto the rheometer plate cooled to 20 °C. Measurements were carried out with a cone plate geometry using a constant oscillation stress of 6.3 Pa. The effect of oscillatory frequency on the dynamic rheological properties of the coacervate network was evaluated at these temperatures after the samples were allowed to equilibrate for 10 min. The mechanical spectra were characterized by observing the in-phase (G') and out-of-phase (G'') storage modulus as function of angular frequency (ω) in the range of 0.1 to 100 rad/s.

DSC experiments were performed by using a DSC 4000 (Perkin-Elmer) instrument. Here, the objective was to determine and correlate the melting temperature of the coacervates and gels with the results obtained from rheology. The endotherms obtained were used to probe coacervate to ion gel phase transition. In a typical experiment, 10 mg of the sample was taken on an aluminum pan and hermetically sealed. The temperature sweep was performed with the heating rate maintained at 5 °C/min. The measurement protocol was as specified by the manufacturer of the instrument.

We adopted Raman spectroscopy to investigate the hydration of coacervates and respective ion gels prepared in aqueous IL solutions because vibrational spectra are very sensitive to the local molecular environment. Raman spectra from all samples were recorded on a FT-Raman Spectrometer

dx.doi.org/10.1021/jp3102089 | J. Phys. Chem. B 2012, 116, 14805–14816

(1064 nm) attached with a Microscope (Varian 7000 FT-Raman and Varian 600 UMA).

III. RESULTS AND DISCUSSION

It is imperative to mention the physical characteristics the biopolymers used prior to undertaking any discussions on their binding features. In an earlier study, we provided a detail account of their physical properties where molecular weight of gelatin A and base pair quantification of DNA were performed using SDS-PAGE and agarose gel electrophoresis methods,[42] respectively. Similarly, the persistence length of GA was estimated from light scattering data. DNA was found to be having 200 base pairs[42] and the persistence length[43,44] ≈50 nm. The measured molecular weight of gelatin A was ≈90 ± 10 kDa, and this chain had a persistence length ≈10 nm. Thus, DNA and gelatin A (GA) had a characteristic charge ratio (DNA:GA = 16:1) and persistence length ratio (5:1). The charge ratio was estimated from their measured ζ potential data. As stated earlier, the experiments were carried out in two distinct steps: first we probed the binding profile of the two biopolymers at a fixed IL but varying protein concentration, and in the second step, we investigated the same at a fixed protein but varying IL concentration.

a. Kinetics of DNA-Gelatin A Binding: Protein Concentration Dependence. Gelatin A (GA) solution was gradually added to the DNA (0.005% (w/v)) solution at room temperature; solution turbidity, viscosity, UV−vis absorption, ζ potential, and hydrodynamic radii of the system formed were monitored systematically. This data are illustrated in Figure 1A, which clearly implies the existence of optimum binding occurring when the GA concentration was 0.1% (w/v). The turbidity of the solution was less than 40% for GA < 0.075% (w/v) and also for GA > 0.125% (w/v). Thus, three distinguishable binding regions prevailed in this system pertaining to GA < 0.075%, 0.075 < GA < 0.125%, and GA > 0.125% (w/v) which we define as regions I, II, and III. Note that the IL concentration was kept fixed at 0.05% (w/v) in all these measurements. It will be shown later that at this concentration IL supported maximum DNA-GA interaction.

The data shown in Figure 1B data are consistent with aforementioned demarcation. A closer examination of region I reveals that in this region as the protein concentration was increased the turbidity increased by 40%, ζ potential decreased from −80 to −5 mV (95%), and hydrodynamic radii of the complex decreased by close to 60%. Thus, the solution contained DNA-IL-GA complexes that had size less than that of pristine DNA, moreover, these complexes carried marginal surface charge. This binding can be described as follows:

$$\mathrm{GA} + [\mathrm{DNA}]_{\mathrm{const}} + [\mathrm{IL}]_{\mathrm{const}} \rightarrow (\mathrm{GA\text{-}IL\text{-}DNA})_{\mathrm{complex}}$$
$$0 < C_{\mathrm{GA}} < 0.075\%\ (\mathrm{w/v}) \qquad (2)$$

We shall refer to this as primary binding between the nucleic acid and the protein molecule mediated by the IL, which resulted in making the DNA molecule compact. It must be realized that the pH of the DNA, GA, and IL interacting solution was 6.0 ± 0.5 where DNA molecules were anionic and protein was cationic ($pI \approx 9.0$). This facilitated strong Coulombic interaction between the biopolymers though limited to screening by the presence of IL molecules.

Condensation of DNA is known to arise from two important mechanisms: phosphate charge neutralization of the DNA molecule and/or reduction of water activity through the reduction in dielectric constant of the medium. Manning's condensation theory clearly explains cation-induced condensation of DNA molecules mostly by neutralizing phosphate charge.[45,46] It was also shown that condensation ensued when ∼80% of the charge was neutralized. Substantial folding of high molecular weight DNA could be observed in presence of polylysine and polyethylene oxide molecules.[47] Interestingly, even nonpolar molecules like polyvinyl pyrrolidinone influence DNA folding.[48] Thus, it is believed that several factors favor DNA condensation and aggregation, in addition to electrostatic forces, which include hydration forces and cross-linking by condensing ligands.[49,50] In the present case it is plausible that DNA and GA molecules bind through a mechanism described by eq 2 where close to 95% charge neutralization was achieved. Thus, if we assume the IL molecules to be counterions to DNA in Manning's model, a double layer of IL molecules will facilitate the formation of the DNA-IL-GA complex, as is shown in Figure 14B with the concomitant condensation of DNA molecule that was evidenced from the reduction in the size data. However, the viscosity data did not reveal any reduction, which is understood as follows. The solution viscosity is a function of molecular weight and shape asymmetry of the solute in a given solution. The binding of DNA to GA significantly increased the molecular weight of the complex that was manifested in the solution viscosity data.

i. Region II Secondary Binding (Complete Charge Neutralization). As the concentration of GA was further increased, the solution properties changed significantly. It is seen from Figure 1B that significant change in solution properties was observed for $0.075 < C_{\mathrm{GA}} < 0.125\%$ (w/v), the turbidity increased 2-fold, ζ potential decreased from −5 to 0 mV (complete charge neutralization) and hydrodynamic radii increased 3-fold. Appearance of charge neutralized soluble complexes and sharp rise in turbidity are signatures of initiation of coacervation,[5−8] which is clearly noticed from the Figure 1 data. This binding mechanism followed the description

$$(\mathrm{GA\text{-}IL\text{-}DNA})_{\mathrm{complex}} + (\mathrm{GA\text{-}IL\text{-}DNA})_{\mathrm{complex}}$$
$$\rightarrow [(\mathrm{GA\text{-}IL\text{-}DNA})_{\mathrm{complex}}\text{-}\mathrm{IL}\text{-}(\mathrm{GA\text{-}IL\text{-}DNA})_{\mathrm{complex}}]$$
$$0.075 < C_{\mathrm{GA}} < 0.125\%\ (\mathrm{w/v}) \qquad (3)$$

In this narrow GA concentration range the protein molecules aggressively bind to DNA facilitated by the presence of IL molecules. Coacervates were extracted in this region from the reaction vessel where the yield was maximum.

ii. Region III Formation of Insoluble Complexes. For $0.125 < C_{\mathrm{GA}} < 0.25\%$ (w/v), the complexes were found to be neutral in charge, turbidity decreased sharply and so was the absorbance, leading to liquid−solid phase separation. The soluble complexes undergo Ostwald ripening to give rise to insoluble complexes and finally lead to precipitation. Here the measured hydrodynamic radii of the complex and viscosity of the solutions reduced with GA concentration. The 900 nm hydrated aggregates constituted coacervate droplets that immediately sedimented to the bottom of the reaction beaker thereby reducing the average size of the complexes, turbidity and polydispersity of the system. However, the residual interactions that were still present continued to drive the formation of larger aggregates, and in a period of another ≈6 h the coacervate droplets again reached a size that ensued another round of sedimentation. As the concentration of available protein aggregates decreased with time, this process slowed

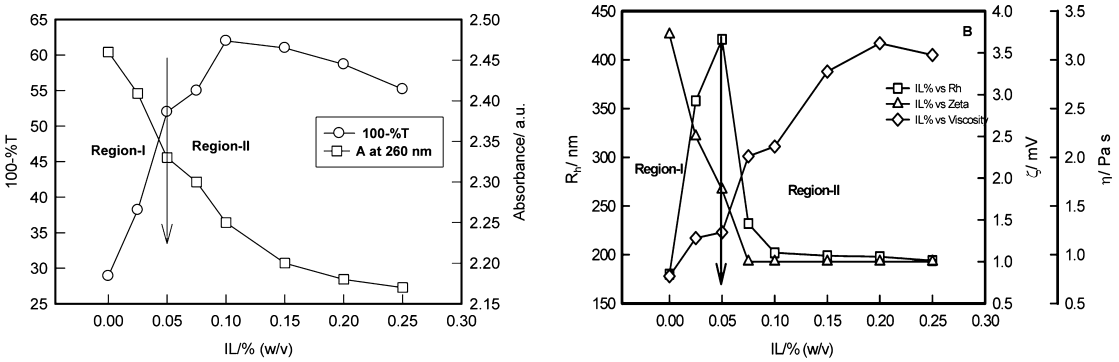

Figure 2. (A) Turbidity (100-%T) and absorbance, A. (B) ζ potential, viscosity, and hydrodynamic radius (R_h) data of the DNA−protein complex as a function of IL concentration. The DNA concentration was fixed at 0.005% (w/v). The GA concentration was fixed at 0.1% (w/v) (neutralization point). Experimental data pertain to 20 °C. Arrows indicate the optimum binding concentration of IL and also separates region I from region II. Solid lines are guides to the eye.

down considerably after a while (≈60 h). This observation revealed that coacervation phenomenon persisted in the supernatant for a long period of time even after the removal of larger aggregates via sedimentation. This was a result of systematic loss of large complexes to phase separation and continuous formation of such complexes from residual soluble aggregates. Such a phenomenon has been reported earlier in protein−protein coacervating solutions.[51]

b. Kinetics of DNA-GA Binding: IL Concentration Dependence. A and B of Figure 2 illustrate the binding profile of the two biopolymers as function of IL concentration where the binding mechanism is clearly seen to be dependent on ionic environment of the solvent. The data in the figures reveal a rapid rise in turbidity and sharp reduction in absorbance in the IL concentration region, 0 < [IL] < 0.05% (w/v). In this region the ζ potential reduced by close to 50% and DNA-IL-GA complexes grew to reveal an apparent hydrodynamic radius ≈400 nm. Correspondingly, the solution viscosity increased by more than 50%. This domain is shown as region I of the binding curve in the aforesaid figures. It must be realized here that the maximum intermolecular binding occurred at [IL] = 0.05% (w/v). Thus, all the DNA-GA binding studies described in section III.a were carried out at this IL concentration.

Further addition of IL facilitated dissociation of large complexes into smaller units with each of these having an apparent size ≈200 nm. These are completely charge neutralized complexes with considerable asymmetry in their geometrical shape, which is revealed from the viscosity data. This, region II, prevailed in the IL concentration region beyond 0.05% (w/v). Increasing the IL concentration beyond 0.1% (w/v) neither facilitated nor inhibited the growth of complexes. It is possible that excess IL molecules formed micelles that coexisted with the soluble complexes.

Thus, in the two regions discussed above, the following equilibrium binding reactions prevailed:

$$\text{Region I: } [\text{GA}]_{\text{const}} + [\text{DNA}]_{\text{const}} + \text{IL} \rightarrow (\text{GA-IL-DNA})_{\text{complex}} \qquad 0 < [\text{IL}] < 0.05\%\ (\text{w/v}) \tag{4}$$

$$\text{Region II: } (\text{GA-IL-DNA})_{\text{complex}} + \text{IL} \rightarrow (\text{GA-IL-DNA})_{\text{complex}} + (\text{micelles})_{\text{IL}} \qquad [\text{IL}] > 0.1\%\ (\text{w/v}) \tag{5}$$

Qualitatively, there was no difference between the binding kinetics occurring in region II of Figure 1 and region I of Figure 2. The differential binding was manifested beyond this binding regime only. However, the binding data in hand implied that maximum binding between the DNA and protein molecule occurred when the IL concentration was ≈0.05% (w/v) and the GA concentration was ≈0.1% (w/v).

c. Temperature Induced Coacervate-Anisotropic Gel Transition. The coacervate samples appeared opaque with a pale yellow coloration when extracted from the reaction vessel. These samples were subjected to slow heating (1 °C/min) in a thermostat up to a maximum temperature 50 °C followed by cooling to room temperature (20 °C). During this protocol, originally opaque looking coacervate samples became optically clear and transparent (Figure S1 of Supporting Information). These were examined for presence of anisotropy by depolarized light scattering. In this experiment, both the vertical and horizontal component of polarized scattered light (633 nm) was measured and depolarization ratio D_p was determined. Depolarization ratio is defined as follows[52]

$$D_p = \frac{I_{VH}}{I_{iso}} \tag{6}$$

and

$$I_{iso} = I_{VV} - \frac{4}{3} I_{VH} \tag{7}$$

where I_{VH} and I_{VV} are the depolarized and polarized components of the scattered intensity. The depolarization ratio is a measure of anisotropy present in the system. In the gel system the depolarization ratio was observed to increase with increase in GA concentration up to 0.15% (w/v) and reached a plateau afterward (Figure 3). For comparison, the depolarization data obtained from an identical sample not containing IL (blank) is also included. Though, the observed optical anisotropy was marginal (<10%) the same was consistently seen for all the ion gel samples.

Coacervates are known to be highly heterogeneous materials containing a hierarchy of length scales that define and distinguish polymer-rich and polymer-poor regions.[53] When such a sample is subjected to slow heating (to 50 °C) followed by cooling to room temperature (20 °C), weakening of the DNA-GA binding occurs that favors preferential GA-GA interaction resulting in the reorganization of labile caocervate material into rigid, self-sorted and anisotropic ion-GA gel with

dx.doi.org/10.1021/jp3102089 | J. Phys. Chem. B 2012, 116, 14805−14816

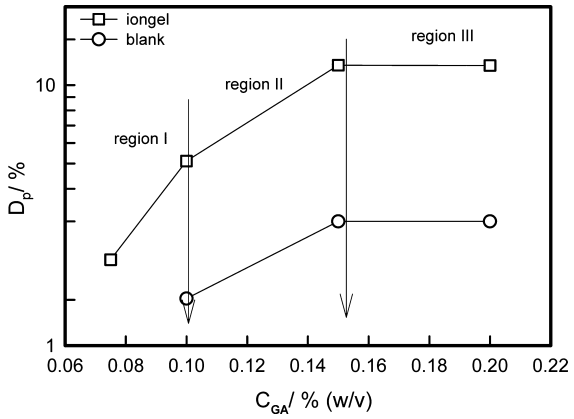

Figure 3. Plot of variation of depolarization ratio (D_P) as function of GA concentration for the ion gel samples derived from heat treated complex coacervates in IL solutions. Here, DNA and IL concentrations were fixed at 0.005 and 0.05% (w/v), respectively. The blank samples did not contain IL. Arrows demarcate the various regions. Solid lines are guides to the eye.

DNA molecules acting as scaffolds. Such a material will be spatially heterogeneous and anisotropic due to preferential alignment of DNA molecules as shown in Figure 14E. We refer to this phase transition as first-order because the process involves enthalpy. Figure S2 (Supporting Information) shows a weak glass-like transition close to 39 °C which requires further probing.

Anisotropic gels[54,55] of liquid crystals are ubiquitous whereas polymer gels rarely exhibit anisotropy. As far as DNA gels are concerned, some observations of anisotropy in specialized systems have been reported in the literature. Furusawa et al.[56] have reported formation of water-insoluble anisotropic gels of salmon milt DNA that was formed in concentrated DNA aqueous borate solutions by interaction with concentrated aluminum chloride. Repressor proteins show highly specific binding to DNA motifs resulting in a bent DNA–protein complex. The rod-like conformation of DNA does exhibit local bending features that are predictable by elastic models that incorporate sequence-dependent anisotropic conformational changes.[57] In our system, the heat induced dissociation of DNA–protein coacervate follow preferential protein–protein aggregation mediated by the ionic liquid, yielding protein ion gels with the rodlike DNA molecules acting as scaffolds. The oriented spatial arrangement of these scaffolds attributed marginal optical anisotropy to this material. This explains the origin of depolarized light scattering data. The schematics are illustrated in Figure 14, which adequately captures the aforesaid binding protocol.

d. Coacervates versus ion gels: Differential Properties. The complex coacervates and their heat induced ion gel samples were examined for their thermo-mechanical properties by SANS, Raman spectroscopy and rheology methods. The SANS data revealed the microscopic structure of the material under consideration over a length scale of a few nanometers, whereas Raman spectra probed the hydration of the chains in their microenvironment and the viscoelastic attributes were captured in rheology studies. The samples were systematically and comprehensively studied using aforesaid array of techniques which is described in the following.

i. Study of Differential Microstructure. The coacervates were extracted from the interacting solutions prepared in deuterated water, having optimum IL concentration and five distinct concentrations of GA, namely, 0.075, 0.10, 0.15, 0.20 and 0.25% (w/v). These samples were subjected to SANS studies to determine their underlying microscopic structures. The static structure factor data is depicted in Figure 4 for various protein concentration of the sample.

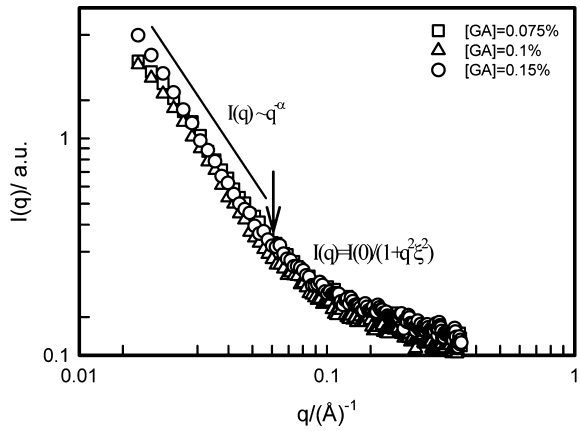

Figure 4. Logarithmic plot of DNA–protein coacervate structure factor, $I(q)$ versus scattering vector q, for three protein concentrations measured by SANS at 20 °C. DNA and IL concentrations were fixed at 0.005 and 0.05% (w/v). Note the invariance of the scattering profile with GA concentration. The arrow demarcates the two scattering regions.

Representative structure factor data for ion gel samples recorded at different temperatures is depicted in Figure 5 for the sample having C_{GA} = 0.1%, DNA = 0.005%, and [IL] = 0.05% (w/v).

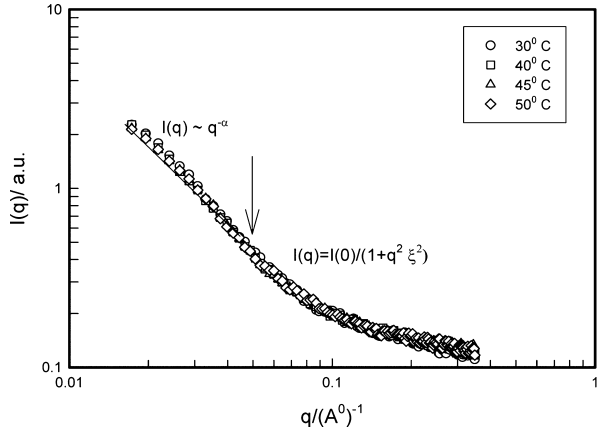

Figure 5. Logarithmic plot of GA ion gel structure factor, $I(q)$ versus scattering vector q, shown for four temperatures. GA, DNA, and IL concentrations were fixed at 0.1, 0.005, and 0.05% (w/v), respectively. Note the marginal dependence of the scattering profile on temperature. The arrow demarcates the two scattering regions.

The scattering profiles depicted in Figure 4 show the SANS data of DNA–protein complex coacervates at three protein concentrations which are remarkably similar and, therefore, appear to be invariant of protein concentration. These data could be split into two distinct regions: (i) for $0.0173 < q < 0.0353$ Å^{-1}, where the data provided excellent least-squares fitting to the power-law function

dx.doi.org/10.1021/jp3102089 | J. Phys. Chem. B 2012, 116, 14805–14816

$$I(q) \sim q^{-\alpha} \quad (8)$$

and (ii) for 0.0353 < q < 0.35 Å^{-1}, where the data could be fitted to the Ornstein–Zernike function[58]

$$I(q) = I(0)/(1 + q^2\xi^2) \quad (9)$$

Here the correlation length of the density–density correlation function is given by ξ, which is related to the mesh size of the material under consideration.

The $I(q)$ vs q profiles depicted in Figures 4 and 5 do convey information about structure factor of coacervate/gel samples. The two q-regions were separated manually by examining the $I(q)$ vs q and $I(q)^{-1}$ vs q^2 plots. A clear change in slope was discernible at q^* = 0.0353. For $q < q^*$, the data was fitted to power-law and for $q > q^*$ to the Ornstein–Zernike function, which yielded robust and reproducible data fitting from sample to sample and within the same sample.

An examination of the neutron scattering length density of the two biopolymers revealed that they were similar. But, the number of protein molecules was far too large as compared to the number of DNA molecules (molecule to molecule number ratio of DNA:GA = 1:15 at the lowest and 1:50 at highest GA concentration). The molecule to molecule number ratio of GA:IL = 1:30 approximately. Thus, most of the neutron scattering owed its origin to protein molecules. The exponent defined by eq 8 owes its origin to the geometry of the scattering moiety in a given system. For instance, α = 1, 1.7, 2, and 4 correspond to geometrical shapes of rod, diffusion limited cluster (DLA), Gaussian coil, and sphere, respectively. For self-similar objects, this exponent is equivalent to the mass fractal dimension of the object. The analysis of SANS data from coacervate yielded α = 1.60 ± 0.2 for C_{GA} = 0.075 and 0.10% (w/v) samples whereas for C_{GA} = 0.15 and 0.20% (w/v) coacervate we found α = 1.8 ± 0.2. For the diffusion limited aggregation (DLA) process it is well-known that α = 1.7. Thus, it is plausible that the coacervate material composed of DLA clusters at room temperature when the protein concentration was <0.1% (w/v). However, at higher protein concentration, α = 1.8 ± 0.2, implying the scattering moieties had Gaussian-like conformation (theoretical value of α = 2). This makes the binding protocol significantly heirarchial.

As has been said earlier, the coacervate material transitted to an ion gel phase upon heating (50 °C) followed by cooling to room temperature (20 °C). The evolution of static structure factor as a function of temperature is illustrated in Figure 5. As in the room temperature case, the scattering profiles overlap revealing remarkable similarity. These data were analyzed exactly as before, which yielded excellent fitting with $\chi^2 > 0.95$. This gave power-law exponent α = 1.5 ± 0.1 independent of temperature, but much smaller than the same observed at room temperature, implying temperature induced reorganization of the coacervate into rarified assembly of protein chains arranged as fractal objects. Such a process would make the material optically clear, which was indeed the case. Figure 6 shows the dependence of the power-law exponent α on protein concentration and temperature. We found the exponent α = 1.6 ± 0.1 for 0.1% (w/v) ion gel independent of temperature, whereas for 0.075 and 0.15% (w/v) ion gels the exponent value reduced to α = 1.1 ± 0.1, indicating preferential scattering originating from rod-like DNA molecules.

The mesh size determined from the experimental data using eq 9 gave ξ = 2 ± 0.1 nm, which was independent of protein concentration. Interestingly, the mesh size remained invariant

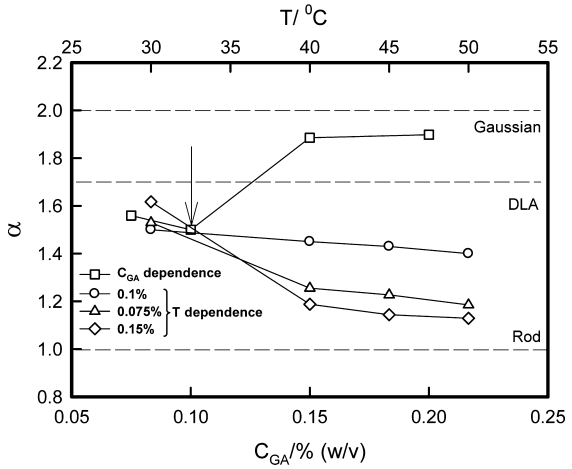

Figure 6. Variation of power-law exponent α defined by eq 8 as function of GA concentration and temperature. Solid lines are guides to the eye. The theoretical value of the exponent for rod-like, DLA, and Gaussian chains is shown as dotted lines. Notice the change in slope (arrow) at $C_{GA} \approx 0.1\%$ (w/v) and the invariance of the exponent with the sample temperature for this ion gel.

of sample temperature also. The persistence length of gelatin A ≈ 10 nm[42] whereas for gelatin B it is ≈2.0 nm.[59,60] Thus, it was intriguing that the observed mesh size was less than the persistence length of the protein chain (GA), which implied that the coacervate and the ion gel phase was composed largely of heavily (physically) cross-linked gelatin chains. However, the present SANS study could not clearly distinguish between the complex coacervate and its heat induced ion gel. This made it imperative to subject these samples to rheology and Raman spectroscopy studies.

The q-range in the power-law regime spreads over a factor of 2 only. Thus, the information content obtained from the data fitting can at best qualify as indicative. The results, thus obtained are summarized in Figure 6 where the specific power-law exponents have been assigned physical meaning. As is seen from this plot, the low concentration protein regime has overlapping exponent values where ambiguity prevails. However, the present study dwells on the observation of a coacervate–anisotropic ion gel phase transition not reported hitherto. The SANS data were used as Supporting Information to distinguish between coacervate and gel which, we believe, the present data serves rather well. A better quality SANS profile will resolve this issue conclusively.

ii. Study of Differential Hydration. Coacervate samples made in D_2O were used for Raman studies too. Even the slightest change in the local molecular environment can be easily sensed by vibrational spectra when the samples are subjected to Raman studies. Raman spectra of DNA-GA complex coacervates in IL solutions are expected to be rich in information and complexity as well because such spectra would not only contain information about various characteristic Raman active modes associated with the biopolymers and IL molecules but also would reflect the various O–D stretching modes pertaining to D_2O molecules. A set of representative spectra is plotted in Figure 7 for GA = 0.1% (w/v) complex coacervate and its respective ion gel. These spectra do not reflect various characteristic Raman active modes associated with IL molecules due to their very low concentration. However, the various O–D stretching modes residing in the frequency region 2000–3000 cm^{-1} dominate the spectra.[61,62]

dx.doi.org/10.1021/jp3102089 | J. Phys. Chem. B 2012, 116, 14805–14816

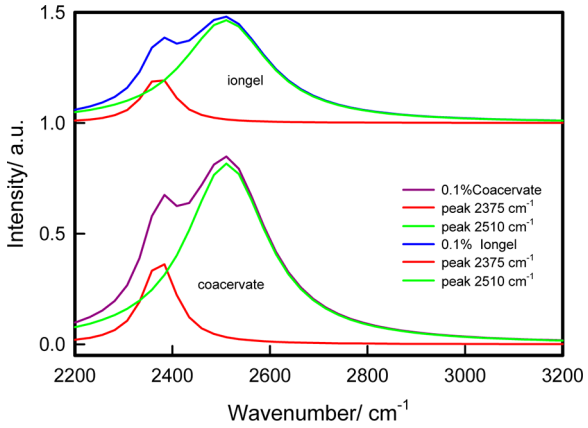

Figure 7. Representative Raman spectra of a coacervate sample and its respective ion gel. Deconvolution yielded two distinct peaks located at frequency 2375 and 2510 cm^{-1} representing vibrational modes of structured and semistructured heavy water.

The Raman spectra were fitted to two-component Lorentzian functions using Origin 6.1 software, which was robust and highly reproducible with the overall statistical error remaining less than typically 2−3%. This procedure yielded two discernible bands in the frequency range 2000−3000 cm^{-1} and the deconvoluted peaks (2375 and 2510 cm^{-1}) are identified as the characteristic vibrational modes of heavy water. The in-phase vibration of OD stretching mode generates the peak at ≈2400 cm^{-1} (here 2375 cm^{-1}). This signifies the structurally arranged heavy water, also referred to as ice like structures. The Raman peak, at 2510 cm^{-1}, in the spectra is identified as C−OD stretch mode. This fraction originates from the partially-structured heavy water.[61,62]

The relative abundance of structured and partially structured D_2O in complex coacervates and its ion gel samples is reflected in the fractional area of the Raman bands located at 2375 and 2510 cm^{-1}, respectively. The same is plotted in Figure 8 for various concentrations of the protein. These data reflect that between 0.10 and 0.15% (w/v) protein concentration there was significant loss in hydration provided by structured D_2O in the

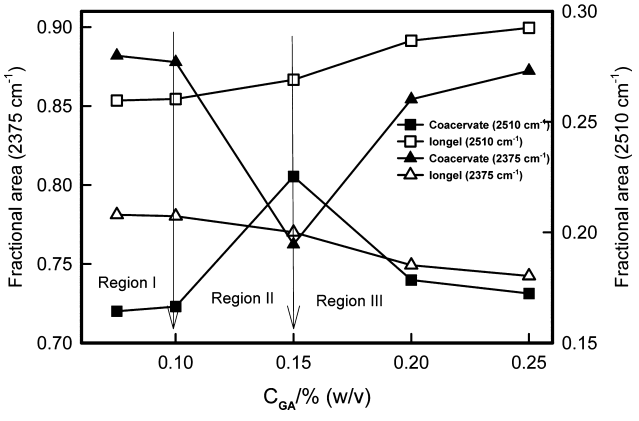

Figure 8. Relative fractional area of 2375 and 2510 cm^{-1} Raman band corresponding to structured and partially structured D_2O in complex coacervates and corresponding ion gels. The regions between the arrows refer to the maximum DNA-GA binding region where hydration changes significantly. Note the relatively weak variance of hydration with protein concentration in ion gels. Arrows demarcate various regions. Solid lines are guides to the eye.

coacervate samples, which was recovered for GA concentration above 0.20% (w/v). In this regime the partially structured water provided necessary hydration to the biopolymers, which is observed from enhanced contribution of the 2510 cm^{-1} band. Thus, in the coacervate samples hydration was strongly protein concentration dependent. In contrast, the ion gels remained preferentially hydrated by partially structured D_2O regardless of the protein concentration.

iii. Study of Differential Viscoelasticity and Melting. The viscoelastic behavior of the samples was probed by rheological studies where the materials were probed for their thermal characteristics (isochronal temperature sweep experiments) and mechanical characteristics (isothermal frequency sweep experiments). Such measurements produce two characteristic elastic modulii, $G'(\omega)$ and $G''(\omega)$, from the data. The storage modulus, $G'(\omega)$, accounts for the energy stored in the system at a given temperature whereas the loss modulus, $G''(\omega)$, quantifies the dissipative loss, and as expected, both of these parameters are dispersive in nature.[63]

Figure 9 illustrates the temperature dependence of the elastic modulii for a 0.1% (w/v) coacervate and ion gel samples. For

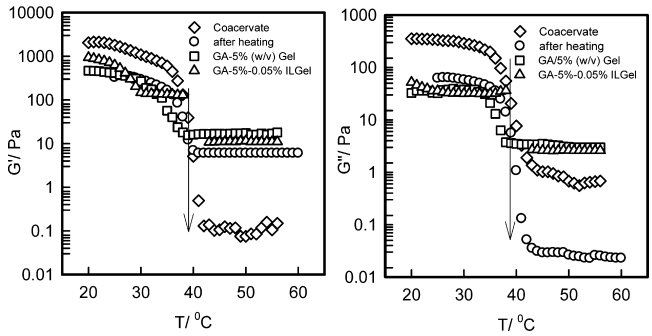

Figure 9. Variation of storage modulus $G'(\omega)$ and loss modulus $G''(\omega)$ of 0.10% GA coacervate, ion gel, GA5% gel, and GA5% gel made in 0.05% (w/v) IL solution shown as function of temperature. Temperature ramp = 1 °C/min at a constant oscillation frequency of 1 Hz was used and a constant strain was maintained at 6.3 Pa during these experiments. Arrows represent the indicative melting temperature T_m.

comparison similar data are obtained from two control samples, GA gel and GA gel made in 0.05% (w/v) IL solution, are also included in this figure.

It was observed that the melting temperature T_m was a function of GA concentration which helped us in constructing a UCST phase diagram. This will be discussed later. To place the T_m values in proper perspective, we performed temperature sweep experiments on a 5% (w/v) GA gel sample and a similar gel sample was made in 0.05% (w/v) IL solution. These data are displayed in Figure 9. The DNA-GA coacervate, its ion gel, GA gel, and GA ion gel all showed meting temperatures close to 37 °C. This behavior was further probed by DSC experiments and the endotherms are depicted in Figures S2 and S3 (Supporting Information). The protein concentration dependence is shown in Figure S4 (Supporting Information), which implies two distinct conclusions: (i) ion gels melted at higher temperature, indicating the presence of stronger cross-links in these materials and (ii) coacervates composed loosely bonded intermolecular complexes that were heterogeneous. These conclusions were reinforced from the dispersion

dx.doi.org/10.1021/jp3102089 | J. Phys. Chem. B 2012, 116, 14805−14816

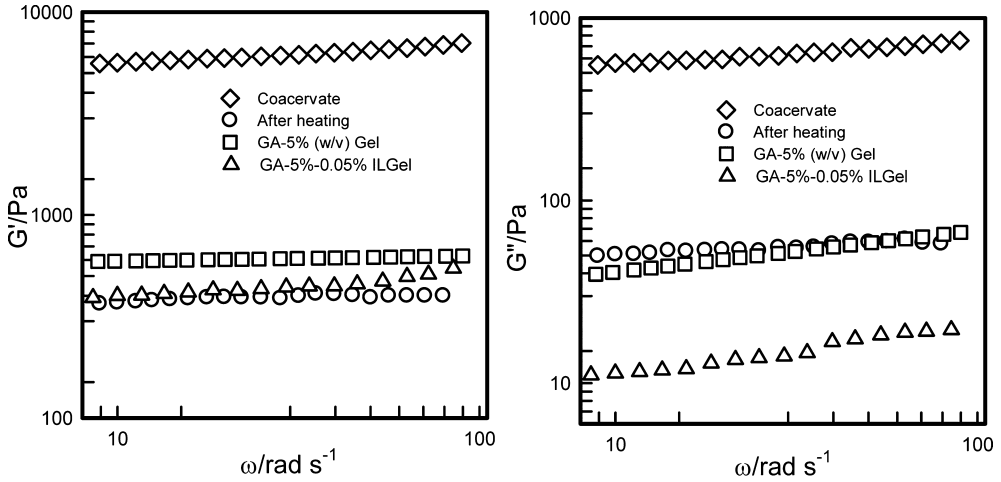

Figure 10. Variation of storage $G'(\omega)$ and loss modulus $G''(\omega)$ of 0.10% GA coacervate, ion gel, GA 5% gel, and GA 5% gel made in 0.05% (w/v) IL solution shown as a function of frequency. The measurements were performed at 20 °C.

behavior data of elastic modulii of these materials, which is discussed below.

Isothermal frequency sweep experiments were carried out to study the frequency dependent behavior of storage and loss modulii $G'(\omega)$ and $G''(\omega)$ at room temperature. The data are shown in Figure 10. The frequency dependence of the elastic modulii was determined by fitting the data to the following functions

$$G'(\omega) = \omega^{n'} \tag{10}$$

$$G''(\omega) = \omega^{n''} \tag{11}$$

Figure 11 depicts the value of the exponents n' and n'' as function of protein concentration which clearly demarcates

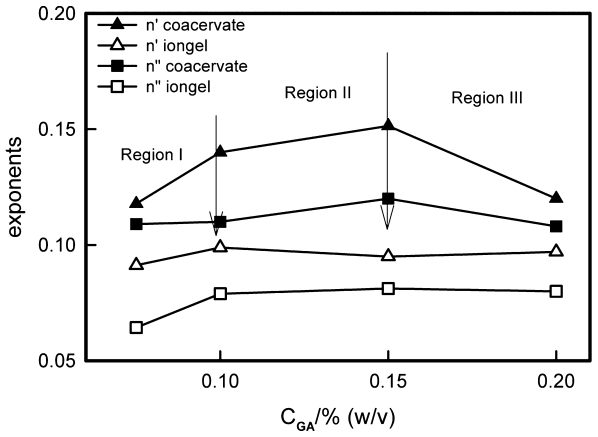

Figure 11. Plot of exponents n' and n'' (eqs 10 and 11) shown as a function of protein concentration. Note that in coacervate samples in region II the exponents were higher compared to other two regions. For ion gel samples, the exponents remained invariant of protein concentration. Arrows indicate various binding regions. Solid lines are guides to the eye.

regions I to III. In region II, the exponents assumed significantly higher values implying strong dispersive behavior. In contrast, the ion gel samples exhibited no dispersion features that clearly indicating their solid-like behavior. Figure 12 shows the loss tangent, $\tan\delta = G''(\omega)/G'(\omega)$, plotted as a function of ω, and the slope of the plots were close to zero. For gels this

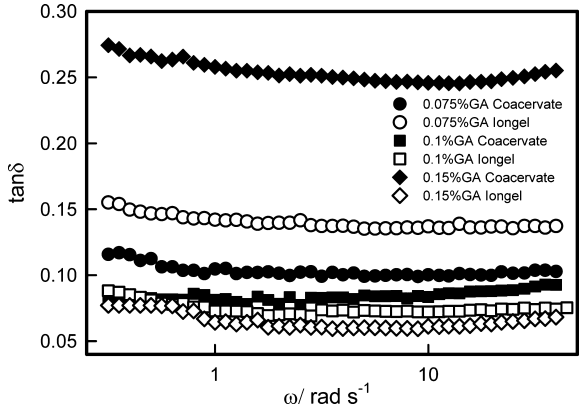

Figure 12. Loss tangent shown for various coacervate and respective ion gel samples. Note the frequency invariance of the loss tangent, which implied that both the coacervate and ion gel states were in anomalous states; neither were these normal gels or polymer melts.

slope is positive, whereas at gelation it is zero and for melts it is negative.[64] Thus, the data indicate that the coacervate phase was located close to phase transition point en route to a gel phase. Heating of the samples (to 50 °C) facilitated a transition to the ion sol, which upon cooling (to 20 °C) yielded the ion gel.

In a network of transiently connected chains, the shear modulus is proportional to the concentration of intermolecular bonds. The value of the length of elastically active strands, calculated from eq 12 is similar to the characteristic viscoelastic network size, ζ_{el}, estimated from the low-frequency shear modulus, G_0. This is a measure of elastic free energy stored per unit volume of a characteristic viscoelastic network of size, ζ_{el}. Hence[65]

$$G_0 k_B T/\zeta_{el}{}^3 \tag{12}$$

Experiments revealed that shear storage modulus of coacervate was weakly dependent on frequency (Figure 10), which reaffirms the validity of eq 12. Thus, typical viscoelastic length scale prevalent in these materials becomes easily accessible from dynamic rheology measurements. The values obtained from the data shown in Figure 13 revealed ζ_{el} residing in the range 12 to 8 nm with a distinct region depicting a plateau with $\zeta_{el} \approx 8$ nm corresponding to GA concentration range 0.10 to 0.15% (w/v)

dx.doi.org/10.1021/jp3102089 | J. Phys. Chem. B 2012, 116, 14805−14816

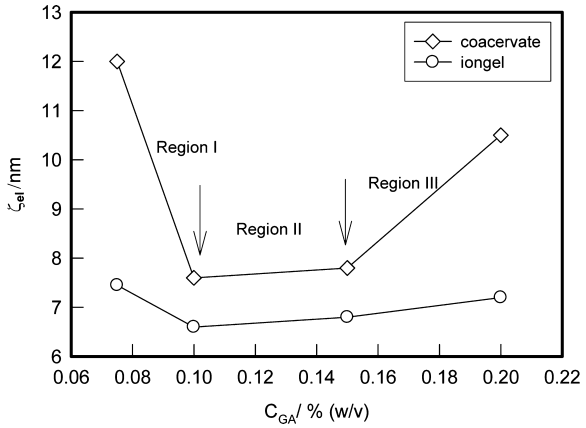

Figure 13. Variation of viscoelastic length, ζ_{el}, as function of GA concentration in coacervate samples and their ion gels. Note that stronger coacervates were formed in the GA concentration range 0.10−0.15% (w/v) whereas for ion gels no preferential GA concentration was observed. Arrows indicate various binding regions. Solid lines are guides to the eye.

(recall that the persistence length of protein is 10 nm). This represents region II of the binding profile where DNA-GA interaction was maximum. This length decreased to 7 ± 0.5 nm for the case of ion gels and was found independent of GA concentration. This clearly indicates that the internal structure of the DNA-IL-GA coacervates and their ion gels are very different with the ion gel capable of storing more elastic energy.

e. Summary of Binding Model and UCST. The data in hand allows us to propose the binding mechanism which is depicted schematically in Figure 14. Figure 1 depicts the kinetics of hierarchical DNA−protein binding and the three binding region demarcated there correspond to the following: region I, C_{GA}< 0.075% (w/v); region II, 0.075 < C_{GA} < 0.125% (w/v); region III, 0.125 < C_{GA} < 0.25% (w/v) (classification I).

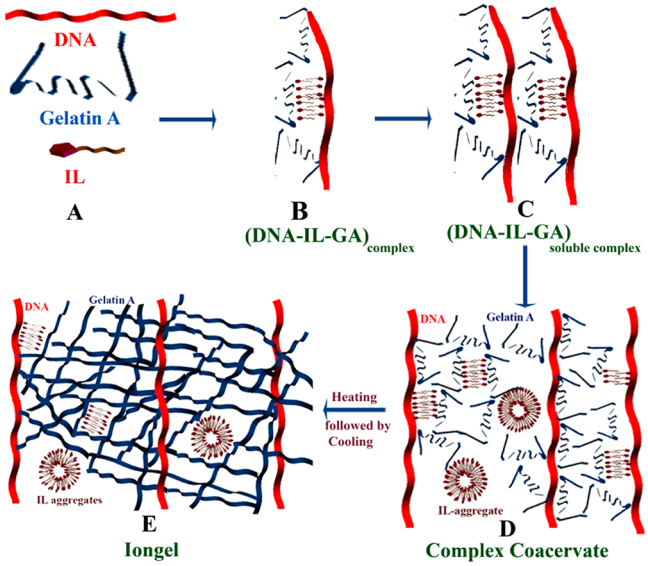

Figure 14. Schematic representation of DNA-GA binding in IL solution. The figure depicts the three distinct interaction regions: (B) condensation of DNA due to primary binding, (C) secondary binding and onset of formation of soluble complexes, and (D) complex coacervation due to Ostwald ripening of soluble complexes. The heat induced ion gel is shown in (E).

However, when we discuss the differential structure properties of coacervates versus their ion gels, we have considered the aforesaid regions to be residing in the protein concentration regimes: region I, C_{GA} < 0.10% (w/v); region II, 0.10 < C_{GA} < 0.15% (w/v); region III, 0.15 < C_{GA} < 0.25% (w/v) (classification II). Thus, there is shift of 0.025% (w/v) of GA concentration in the definition of the two classifications. Such a difference is considered normal because the data presented in Figure 1 are instantaneous values whereas the structure−property data presented in Figures 6−13 pertain to systems that had equilibrated over several days. Thus, we believe that classification II provides a robust and exact hierarchy of DNA−protein binding.

Binding between DNA and GA was facilitated to the maximum limit when the IL concentration was 0.05% (w/v). Keeping this fixed as the GA concentration was increased strong electrostatic interaction between DNA and GA molecules led to the formation of $(DNA\text{-}IL\text{-}GA)_{complex}$, yielding substantial charge neutralization of the nucleic acid. This caused the DNA molecule to condense as per Manning's model (Figure 14B, referred to as region I). Further addition of protein increased the propensity of the $(DNA\text{-}IL\text{-}GA)_{complex}$ structures, thereby increasing the turbidity, absorbance, and viscosity of the solution. Consequently, multiple units of $(DNA\text{-}IL\text{-}GA)_{complex}$ bind to generate charge neutralized soluble complexes that are precursors to coacervation transition (Figure 14C, referred to as region II). A further increase in GA concentration accelerated the growth of soluble complexes, Ostwald ripening ensued, and the onset of complex coacervation was observed (Figure 14D). At higher protein concentration, the region had the signature of low turbidity, reduced absorbance, and smaller soluble complex size (large complexes phase separate).

The heated coacervates facilitated a phase transition from the heterogeneous complex coacervate to anisotropic ion gel where the gel matrix primarily composed of protein molecule with the DNA strands acting as scaffolds (Figure 14E). The complex coacervate and its ion gel had remarkable difference in their physical properties as shown in Table 1. The melting temperature of ion gels as a function of protein concentration allowed us to construct a phase diagram with well-defined UCST. This is illustrated in Figure 15. To the best of our knowledge this is the first time UCST has been experimentally observed for any complex coacervate system. Any phase state exhibiting UCST is associated with increase in second virial

Table 1. Summary of Physical Characteristics Describing Various Condensed Phases of Complex Coacervate and Ion Gel[a]

Sl no.	parameter/property	complex coacervate	ion gel
1	mesh size	2.0 nm	2.0 nm
2	viscoelastic length	8.0 nm	6.5 nm
3	molecular assembly	fractal and Gaussian	fractal
4	optical feature	opaque	clear
5	viscoelastic feature	viscoelastic	elastic
6	hydration	structured water	semistructured water

[a]Data reported pertain to 20 °C for samples prepared in aqueous medium (D_2O for SANS experiments).The transition temperatures are associated with an uncertainty of ±0.5 °C and the same with characteristic sizes is ±5% of the listed data, typically. Data presented are representative and pertain to GA = 0.10% (w/v).

dx.doi.org/10.1021/jp3102089 | J. Phys. Chem. B 2012, 116, 14805−14816

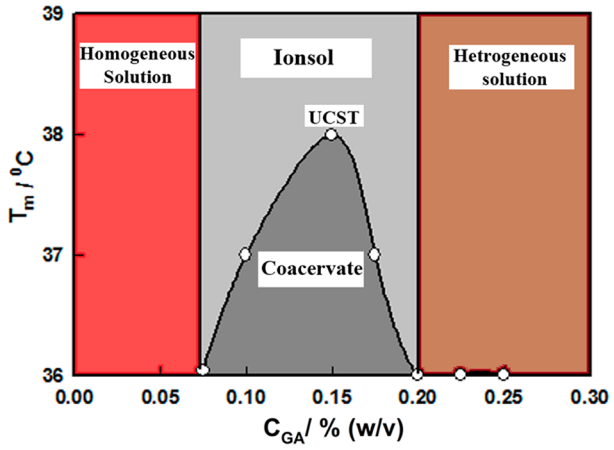

Figure 15. Phase diagram of DNA−GA complex coacervate in ionic liquid solution exhibiting a clear UCST behavior. Solutions were homogeneous and stable at low protein concentration and heterogeneous and unstable at high protein concentration, and the two regions are separated by the coacervate domain. The coacervates upon heating (to 50 °C) exhibited first-order phase transition first to ion sols, and then to ion gels on cooling (to 20 °C).

coefficient of osmotic pressure (A_2) and concurrent decrease in Gibb's free-energy of mixing ($-\Delta G_m$).[66] When this is translated to our case, it would imply increase in protein concentration to increase in A_2 and decrease in $-\Delta G_m$ value.

IV. CONCLUSION

We have performed a systematic and comprehensive study to probe the binding protocol of DNA with a low charge density protein in ionic liquid solutions. The binding profile exhibited optimum binding condition was facilitated when the protein concentration was between 0.10 and 0.15% (w/v) in IL solutions having ionic liquid concentration 0.05% (w/v). The protein concentration dependent hierarchical binding facilitated DNA folding at low, complex coacervation at intermediate and phase separation at high protein concentration. When the coacervate samples were slowly heated to ≈50 °C followed by cooling to room temperature (to 20 °C), a first-order phase transition to an anisotropic ion gel state was observed. The ion gel yielded depolarized light scattering, implying weakening of the DNA-GA binding and preferential GA-GA interaction resulting in the reorganization of labile caocervate material into rigid, self-sorted, and anisotropic ion gel with DNA molecules acting as scaffolds. Rheological studies revealed the coacervate phase residing close to the gelation boundary, which facilitated crossover to the gel state upon slow heating (to 50 °C) followed by cooling to room temperature (to 20 °C).

It is interesting to observe that coacervates and ion gels share a generality as far as their microscopic internal structures are concerned, which is clearly evident from the data shown in Table 1. The optical, viscoelastic, and hydration properties were distinctively different. Thus, it will be appropriate to argue that the internal structure of the heterogeneous coacervate material is composed of cross-linked polymer-rich zones separated by polymer-poor regions having characteristic high viscoelastic length. Such systems are associated with two characteristic relaxation processes: one due to concentration fluctuation and another arising from viscoelastic relaxation. This has been adequately described by models and supported by experiments in the past. Thus, the coacervate phase was in a dynamically evolving state that makes this system extremely interesting. The results presented provide a significant insight into the distinctive microscopic features of these complex coacervates of DNA and gelatin in ionic liquid solutions. This paper does not answer all the questions related to the microstructure of coacervates due to the instrumental limitation of the SANS spectrometer used. For instance, long wavelength concentration fluctuations did not contribute to the neutron scattering profile. Similarly, strong incoherent scattering did not permit explicit examination of the Porod region. Regardless, the plurality and propensity of data in hand allowed us to formulate a deeper understanding of DNA−protein interaction in ionic liquid environment.

■ ASSOCIATED CONTENT

Ⓢ Supporting Information

DSC thermograms, melting temperature data, and photographs of coacervate and ion gel samples. This material is available free of charge via the Internet at http://pubs.acs.org.

■ AUTHOR INFORMATION

Corresponding Author

*E-mail: bohi0700@mail.jnu.ac.in. Tel: +91 11 2670 4637. Fax: +91 11 2674 1837.

Notes

The authors declare no competing financial interest.

■ ACKNOWLEDGMENTS

K.R. is thankful to council of scientific and industrial research, India, for a senior research fellowship. We are thankful to the Advanced Research Instrumentation Facility of the University for allowing us access to the Raman instruments. This work was supported by a research grant under IUC-DAE-CSR Program of Government of India.

■ REFERENCES

(1) Bungenberg de Jong, H. G. In *Colloid Science*; Kruyt, H. R., Ed.; Elsevier: New York, 1994; Chapter III.
(2) Tsuchida, E.; Abe, K. *Interaction between Macromolecules in Solution and Intermacromolecular Complexes*: Springer, Berlin, 1982.
(3) Wang, Y.; Gao, J. Y.; Dubin, P. L. *Biotechnol. Prog.* **1996**, *12*, 356−362.
(4) Dubin, P. L.; The, S. S.; McQuigg, D. W.; Chew, C. H.; Gans, L. M. *Langmuir* **1989**, *5*, 89−95.
(5) Kayitmazer, A. B.; Bohidar, H. B.; Mattison, K. M.; Bose, A.; Sarkar, J.; Hashimoto, A.; Russo, P. S.; Jaeger, W.; Dubin, P. L. *Soft Matter* **2007**, *3*, 1064−1076.
(6) Kaibara, K.; Okazaki, T.; Bohidar, H. B.; Dubin, P. L. *Biomacromolecules* **2000**, *1*, 100−107.
(7) Mohanty, B.; Bohidar, H. B. *Biomacromolecules.* **2003**, *4*, 1080−1086.
(8) Gupta, A. N.; Bohidar, H. B. *J. Chem. Phys.* **2006**, *125*, 054904−1−054904−7.
(9) Burgess, D. J. *J. Colloid Interface Sci.* **1990**, *140*, 227−238.
(10) Smith, A. E. *Science* **1967**, *214*, 1038−1040.
(11) Stewart, R. J.; Wang, C. S.; Shao, H. *Adv. Colloid Interface Sci.* **2011**, *167*, 24−37.
(12) Overbeek, J. T. G.; Voorn, M. J. *J. Cell. Comput. Phys* **1957**, *49*, 7−26.
(13) de Vries, R. *Biochimei* **2010**, *92*, 1715−1721.
(14) Clark, D. J.; Kimura, T. *J. Mol. Biol.* **1990**, *211*, 883−896.
(15) Widom, J. *Annu. Rev. Biophys. Biomol. Struct.* **1998**, *27*, 285−327.
(16) Clausell, J.; Happel, N.; Hale, T. K.; Doenecke, D.; Beato, M. *PLoS ONE* **2009**, *4*, e0007243−1- 14.
(17) Nguyen, T. T.; Shklovskii, B. I. *Physica A* **2001**, *293*, 324−338.

(18) Zhang, R.; Shklovskii, B. I. *Physica A* **2005**, *352*, 216−238.
(19) Castelnovoa, M.; Joanny, J. F. *Eur. Phys. J. E* **2001**, *6*, 377−386.
(20) Kizilay, E.; Kayitmazer, A. B.; Dubin, P. L. *Adv. Colloid Interface Sci.* **2011**, *167*, 24−37.
(21) Baulin, V. A.; Trizac, E. *Soft Matter* **2012**, *8*, 2755−2769.
(22) Ou, Z.; Muthukumar, M. *J. Chem. Phys.* **2006**, *124*, 154902−1−11.
(23) Bordi, F.; Sennato, S.; Truzzolillo, D. *J. Phys.: Condens. Matter* **2009**, *21*, 203102−1−26.
(24) Dobrynina, A. V.; Rubinstein, M. *Prog. Polym. Sci.* **2005**, *30*, 1049−1118.
(25) Sennato, S.; Truzzolillo, D.; Bordi, F. *Soft Matter* **2012**, *8*, 9384−9395.
(26) Capito, R.; Azevedo, H.; Velichko, Y.; Mata, A.; Stupp, S. *Science* **2008**, *319*, 1812−1816.
(27) Biesheuvel, P. M.; Mauser, T.; Sukhorukov, G. B.; Mohwald, H. *Macromolecules* **2006**, *39*, 8480−8486.
(28) Martens, A. A.; van der Gucht, J.; Eggink, G.; de Wolf, F. A.; Cohen Stuart, M. A. *Soft Matter* **2009**, *5*, 4191−4197.
(29) Lemmers, M.; Sprakel, J.; Voets, I.; van der Gucht, J.; Cohen Stuart, M. *Angew. Chem., Int. Ed.* **2010**, *49*, 708−711.
(30) Marsh, K. N.; Brennecke, J. F.; Chirico, R. D.; Frenkel, M.; Heintz, A.; Magee, J. W.; Peters, C.; Rebelo, L. P. N.; Seddon, K. R. *Pure Appl. Chem.* **2009**, *81*, 781−828.
(31) Wassercheid, P.; Keim, W. *Angew. Chem., Int. Ed.* **2008**, *39*, 3772−3789.
(32) Martins, M. A. P.; Frizzo, C. P.; Moreira, D. N.; Nilo, Z.; Bonacorso, H. G. *Chem. Rev.* **2008**, *108*, 2015−2050.
(33) Hagiwara, R.; Ito, Y. *J. Fluorine Chem.* **2008**, *105*, 221−227.
(34) Ohno, H.; Fukumoto, K. *Acc. Chem. Res.* **2007**, *40*, 1122−1129.
(35) Kumar, V.; Malhotra, S. V. *ACS Symp. Ser.* **2010**, *1038*, 91−102.
(36) Rawat, K.; Bohidar, H. B. *J. Mol. Liq.* **2012**, *169*, 136−143.
(37) Anderson, E. B.; Long, T. E. *Polymer* **2010**, *51*, 2447−2454.
(38) Rawat, K.; Bohidar, H. B. *J. Phys. Chem. B* **2012**, *116*, 11065−11074.
(39) Ohshima, H. *Adv. Colloid Interface Sci.* **1995**, *62*, 189−235.
(40) Evans, F. D.; Wennerstrom, H., *The colloidal domain where physics, chemistry and biology meet*; Wiley VCH: New York, 1999.
(41) Aswal, V. K.; Goyal, P. S. *Curr. Sci. India* **2000**, *79*, 947−953.
(42) Arfin, N.; Bohidar, H. B. *J. Phys. Chem. B* **2012**, *116*, 13192−13199.
(43) Mrevlishvili, G. M.; Svintradze, D. V. *Int. J. Biol. Macromol.* **2005**, *35*, 243−245.
(44) Eisenberg, H. *Acc. Chem. Res.* **1987**, *20*, 276−282.
(45) Arscott, P. G.; Ma, C.; Wenner, J. R.; Bloomfield, V. A. *Biopolymer* **1995**, *36*, 345−364.
(46) Marquet, R.; Houssier, C. *J. Biomol. Struct. Dynam.* **1991**, *9*, 159−167.
(47) Lerman, L. S. *Proc. Natl. Acad. Sci. U. S. A.* **1971**, *68*, 1886−1890.
(48) Rau, D. C.; Parsegian, V. A. *Proc. Natl. Acad. Sci. U. S. A.* **1984**, *81*, 2621−2625.
(49) Rau, D. C.; Parsegian, V. A. *Biophys. J.* **1992**, *61*, 246−259.
(50) Schellman, J. A.; Parthasarathy, N. *J. Mol. Biol.* **1984**, *175*, 313−329.
(51) Tiwari, A.; Bindal, S.; Bohidar, H. B. *Biomacromolecules* **2009**, *10*, 184−189.
(52) Barnes, B. J.; Pecora, R. *Dynamic light Scattering*; Wiley Interscience: New York, 1976.
(53) Mohanty, B.; Aswal, V. K.; Kohlbrecher, J.; Bohidar, H. B. *J. Polym. Sci., Part B: Polym. Phys.* **2006**, *44*, 1653−1667.
(54) Guan, Li; Zhao, Yue. *Chem. Mater.* **2000**, *12*, 3667−3673.
(55) Ren, H.; Wu, Shin-Tson. *Appl. Phys. Lett.* **2002**, *81*, 1432−1435.
(56) Furusawa, K.; Minamisawa, Y.; Toshiaki, D.; Takao, Y. *Soft Matter* **2009**, *7*, 132−149.
(57) Gromiha, M. M.; Munteanu, M. G.; Simon, I.; Pongor, S. *Biophys. Chem.* **1997**, *69*, 153−160.
(58) De Gennes, P. G. *Scaling Concepts in Polymer Physics*; Cornell University Press: Ithaca, NY, USA, 1985.
(59) Gupta, A. N.; Mohanty, B.; Bohidar, H. B. *Biomacromolecules* **2005**, *6*, 1623−1627.
(60) Pezron, I.; Djabourov, M.; Leblond, J. *Polymer* **1991**, *32*, 3201−3210.
(61) Walrafen, G. E.; Yang, W.; Chu, Y. C.; Hokmabadi, M. S. *J. Phys. Chem.* **1996**, *100*, 1381−1391.
(62) Dheer, M. K.; Madhavan, D.; Ramachandra Rao, D. *Chem. Phys. Lett.* **1975**, *32*, 341−344.
(63) Ferry, J. D. *Viscoelastic Properties of Polymers*; John Wiley: New York 1961.
(64) Barnes, H. A. *Handbook of Elementary Rheology*; University of Wales Press: Wales, 2000.
(65) Ajji, A.; Choplin, L. *Macromolecules* **1991**, *24*, 5221−5223.
(66) Flory, P. T., *Principles of Polymer Chemistry*; Cornell University Press: Ithaca, NY, USA, 1953.